PAPER

Check for updates

Development of photoluminescent hydrogen-bonded frameworks based on pyromellitic diimide-tethered carboxylic acid hosts and multi-bonding solvent guests†

Raju Ram Puniya,‡[a] Priyanka Takhar,‡[a] Monika Chhapoliya,[a] Rinki Deka,[b] Dhruba Jyoti Kalita [ID][b] and Devendra Singh [ID] *[a]

The significance of hydrogen-bonding interactions in improving the chemical and physical properties of functional materials related to sustainable energy, gas absorption, catalysis, and pharmaceuticals has gained considerable research attention. In this report, some unprecedented hydrogen bond motifs between the −COOH group and the solvents capable of forming multiple hydrogen bonds with −COOH are studied. The effects of such diverse motifs on the construction of 3D supramolecular architectures of hydrogen-bonded host–guest frameworks and their optical properties are elucidated. For this purpose, structural studies on seven solvates, namely, **1a** (**1**:2DMF), **1b** (**1**:2pyridine), **1c** (**1**:2quinoline), **2a** (**1**:2DMF), **2b** (**1**:2pyridine), **2c** (**1**:2quinoline), and **2d** (**1**:1quinoline:2piperidine), of two isomeric pyromellitic diimide hosts **1** and **2** were carried out. Single crystal X-ray diffraction (SCXRD) analyses revealed that solvates **1a**, **2a**, and **2b** show 3D non-porous supramolecular host–guest networks, whereas solvates **1b**, **1c**, **2c**, and **2d** show 3D supramolecular host–guest channelled architectures accommodating guest solvent molecules within the cavities of different dimensions. Formation of different hydrogen bond motifs, either cyclic/ring (R) or discrete (D) or a combination of both, between the −COOH groups of isomeric hosts and identical guest molecules is analysed through density functional theory (DFT) calculations. Minor differences in the interaction energies of different motifs of isomeric hosts with the same guest suggest that the formation of either motif depends on the steric orientations of hosts and other weak host–guest interactions in the crystal lattices. Solid state fluorescence emission properties of solvates **1a**, **2a**, and **2b** are found to be similar to their respective hosts, whereas those of solvates **1b**, **1c**, **2c**, and **2d** are different from their hosts. Along with the diversity of supramolecular synthons, frontier molecular orbital (FMO) analysis of hydrogen-bonded model structures explained well the different emission behaviours of solvates. Thermal analyses for the solvates are in good agreement for the association of the numbers of guest solvent molecules with both the isomeric hosts. Overall, this research is focused on establishing the phenomena for the formation of distinct hydrogen bond patterns between the two similar host–guest binding groups together with the effect of supramolecular states on the photophysical properties of such hydrogen-bonded complexes.

Introduction

Non-covalent intermolecular interactions play an important role in the organization of molecular assemblies for the development of new functional materials.[1–4] Hydrogen bonds in

combination with other weak interactions, such as π–π, CH–π, van der Waals and charge transfer interactions, facilitate the formation of extended molecular assemblies with novel properties.[5–8] The significance of such weak interactions in the construction of fascinating supramolecular assemblies, such as hydrogen-bonded organic frameworks (HOFs), with potential applications in the fields of gas adsorption and separation,[9–11] fluorescent sensing,[12–14] catalysis,[15–17] proton conduction,[18,19] and biological relevance[20,21] is well documented. HOFs are constructed entirely *via* intermolecular interactions between the molecular units and are considered superior crystalline porous materials than metal–organic frameworks

[a] *Department of Chemistry, Mohanlal Sukhadia University, Udaipur-313001, Rajasthan, India. E-mail: dsingh@mlsu.ac.in*

[b] *Department of Chemistry, Gauhati University, Guwahati-781014, Assam, India*

(MOFs) and covalent-organic frameworks (COFs) owing to their unique features.[22–25] Indeed, multi-component hydrogen-bonded host–guest frameworks, such as cocrystals, salts, solvates or hydrates, also offer advantages in terms of solubility, crystallinity, self-repairing ability, easy reproducibility, bioavailability, and mechanical properties over the distinctive crystalline materials.[26–28] The derivatives of some multiple hydrogen bond donor/acceptor groups, such as carboxylic acid (–COOH),[29] sulfonic acid (–SO$_3$H),[30] amine (–NH$_2$),[31] amidine (–CNHNH$_2$),[32] diaminotriazine (DAT),[33] benzimidazolone,[34] pyrazole,[35] pyridine,[36] and urea,[37] have been reported to construct stable multi-component HOFs so far.

The –COOH group, in conjunction with π–π and CH–π interactions of aromatic units, facilitates the formation of various supramolecular aggregates via dimeric, discrete, or charge-assisted interactions.[38–41] An efficient study on these weak interactions provides scope to improve the properties and applications of active pharmaceutical ingredients,[42] gas adsorbents,[43] catalysts,[44] sensors,[45] receptors,[46] and optical materials.[47] For instance, slight variations in the host–guest hydrogen bond patterns in such multi-component systems lead to supramolecular isomerism, which results in the formation of polymorphs of particular scientific interest.[48] The supramolecular features associated with the –COOH group connected to pyromellitic diimide (PMDI) and naphthalene diimide (NDI) building blocks make them attractive for such studies.[49–52] In these systems, free rotation of cyclic imide ring around the C–N bond arranges hosts and guests in several orientations to facilitate the formation of dissimilar motifs between the –COOH group of host and same guest molecule containing multiple donor/acceptor hydrogen bonding sites. In this

respect, minor differences in the hydrogen bond interactions between the *N,N′*-bis(benzoic acid)naphthalene diimide host and pyridine guest resulted in the formation of polymorphic solvates.[53] A series of inclusion compounds of *N,N′*-bis(gly-cinyl)pyromellitic diimide host with aromatic hydrocarbon guests was also reported to exist via charge transfer and π–π interactions.[54] In our recent study, the formation of two types of hydrogen bond motifs (D or R) between the identical interacting groups of two isomeric host PMDI molecules and some different guest solvent molecules, respectively, was explored using both experimental and theoretical investigations.[55]

Herein, with the objectives to rationalize hydrogen bonding patterns (as illustrated in Scheme 1) between the –COOH group and some multiple hydrogen bonds donor/acceptor groups, seven multi-component host–guest frameworks/solvates of PMDI carboxylic acid hosts (**1** and **2**) with different guest solvents are prepared (Scheme 2), and various types of intermolecular interactions responsible for the formation of their 3D supramolecular architectures are studied. In some of these supramolecular systems, the encapsulation of guests occurs through the creation of primary self-assembly of host molecules, whereas in other structures, the interaction of a host with a guest creates a secondary assembly for guest encapsulation. Unlike in our previous studies, where the D or R binding modes between a single –COOH group and a single guest molecule were analysed, some new and unexplored binding modes of a single –COOH group of host molecules with several guests, viz. DMF and pyridine, are analysed in this study. The photoluminescence properties of such systems are explored based on supramolecular interactions in the structures of solvates and
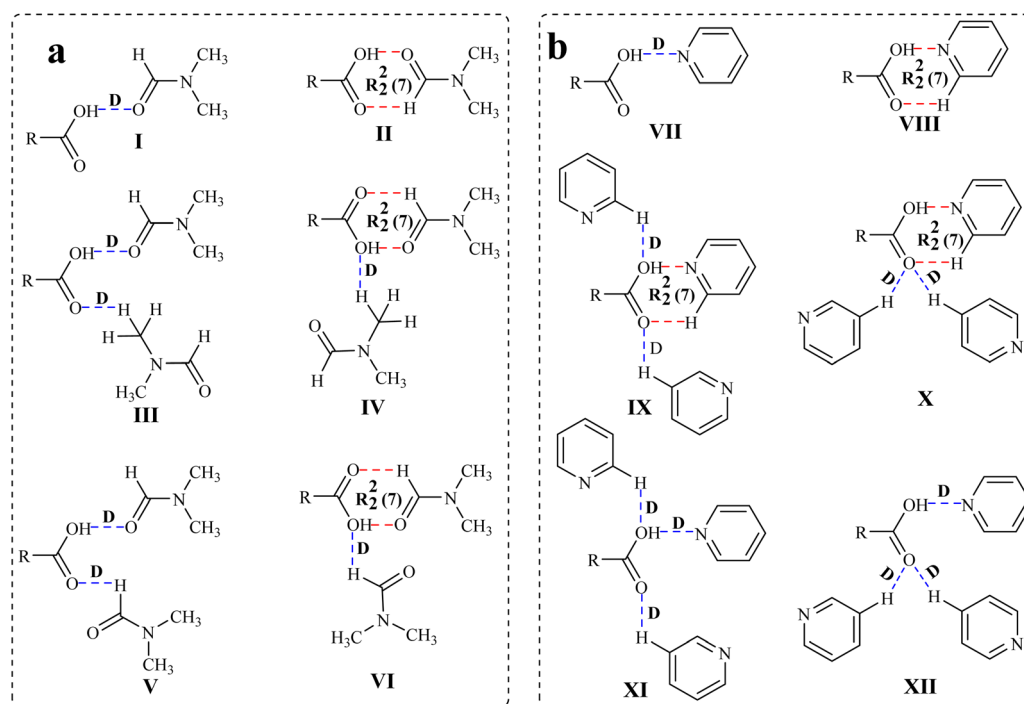
Scheme 1 Illustration of the possible hydrogen bond motifs between (a) the –COOH group and DMF and (b) the –COOH group and pyridine in the structures of the solvates.
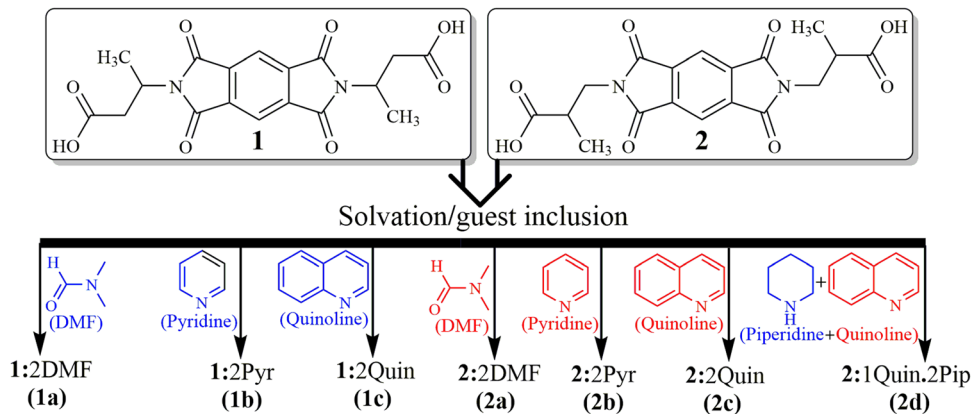
Scheme 2 Structures of hosts **1** and **2** together with guest solvent molecules and host−guest complexes showing host−guest stoichiometry.

FMO analyses of optimized model structures. It is believed that the results of this study will provide insight into the establishment of some newly exposed hydrogen bond motifs in the crystal lattice of solid-state materials.

Results and discussion

The host compounds *N,N′*-bis(butanoic acid)pyromellitic diimide (**1**) and *N,N′*-bis(2-methylpropanoic acid)pyromellitic diimide (**2**) are synthesized by acid anhydride-amine condensation reactions, and their solvates are prepared using the respective solvents for further studies. Except for the crystals of mixed solvate **2d** grown from the quinoline solution of **2** in the presence of piperidine in a 1:1:2 host−guest ratio, all other solvates are prepared by crystallizing host compounds **1** and **2** from the solutions of single solvent, *viz.* DMF, pyridine and quinoline solvents, respectively, in a 1:2 host−guest ratio (Scheme 2). The crystals of suitable diffraction quality could not be obtained for the mixed quinoline and piperidine solvate of host **1**. All the solvates are characterized using various spectroscopic techniques, including FT-IR, NMR, solid state UV-visible and fluorescence emission, thermogravimetric analysis (TGA), differential scanning calorimetry (DSC), powder X-ray diffraction (PXRD) and single crystal X-ray diffraction (SCXRD). The formation of different types of hydrogen bond motifs in the solvates of hosts **1** and **2** with the same solvents (Scheme 1), namely, motifs **III** and **IV** (in DMF solvates **1a** and **2a**), and **IX** and **X** (in pyridine solvates **1b** and **2b**), are analysed by DFT calculations by optimizing formic acid–DMF and formic acid–pyridine molecules as model structures. In addition, the possibility of the formation of slightly different motifs between the –COOH group and the DMF/pyridine molecules (**V**, **VI/XI**, and **XII**), which are not observed in the solvates of DMF and pyridine, is also checked by applying optimized model structures. The purpose of using such model structures was to avoid the complexity of other interactions between the larger hosts so that interactions between the –COOH group and choice of solvent molecules could be analysed clearly. The HOMO–LUMO band gaps of such model structures are also considered to understand the different emission behaviours of DMF and pyridine solvates of

the same host. In this study, the guest quinoline molecules are found to attach with the –COOH groups of host molecules only *via* a similar D mode in the structures of quinoline solvates. Therefore, the formic acid-quinoline models are not considered to conduct theoretical studies. Various intermolecular interactions such as OH–O, OH–N, CH–O, CH–π, CO–π, O–π and short H–H contacts were found to be responsible for the formation of 3D host–guest supramolecular architectures of these solvates.

Analyses of crystal structures and DFT calculations

SCXRD structural analysis shows that solvate **1a** crystallizes in a monoclinic $P2_1/n$ space group and emerges as half of host molecule **1** along with a guest DMF molecule in its crystallographic asymmetric unit. In the crystal lattice of **1a**, the guest DMF molecule interacts with the –COOH group of the host *via* discrete acceptor OH–O (O3–H3···O1D, $d_{D···A}$ 2.6 Å, ∠ D–H···A 170°) and discrete donor CH–O (C2D–H2D3···O4, 3.53 Å, 168.3°) interactions (Fig. 1). It also interacts with the carbonyl oxygen of the cyclic imide ring of the host molecule *via* discrete donor C1D–H1D···O1 (3.36 Å, 173.9°) contact. Further, the host molecules are also found to interact with each other *via* C8–H8B···O3 (3.64 Å, 170°), O2···π (3.1 Å) and O4···π (3.0 Å) interactions, overall constructing a helical 3D host–guest network in which layers of single helix are arranged over each other, as viewed along the *c* axis.

Solvate **2a** crystallizes in the monoclinic $P2_1/c$ space group. It appears as half of host molecule **2** lying on the inversion centre in its crystallographic asymmetric unit along with a guest DMF molecule. Contrary to the structure of **1a**, in the structure of **2a**, the guest DMF molecule interacts with the –COOH group of the host by the combination of acceptor OH–O (O3–H3···O1D, $d_{D···A}$ 2.58 Å, ∠ D–H···A 170.9°) and donor CH–O (C1D–H1D···O4, 3.2 Å, 124.5°) interactions, making a cyclic $R_2^2(7)$ motif along with a discrete donor C3D–H3D3···O3 (3.64 Å, 161.9°) interaction (Fig. 2). It interacts similarly with the carbonyl oxygen of the cyclic imide ring of the host molecule *via* C2D–H2D1···O2 (3.6 Å, 159.2°) contact. The host molecules also interact with each other *via* C3–H3···O1 (3.27 Å, 128.5°) and C9–H9A···O2 (3.57 Å, 166.4°) interactions and stack over each other to create a 2D layered pattern along the *b* axis.
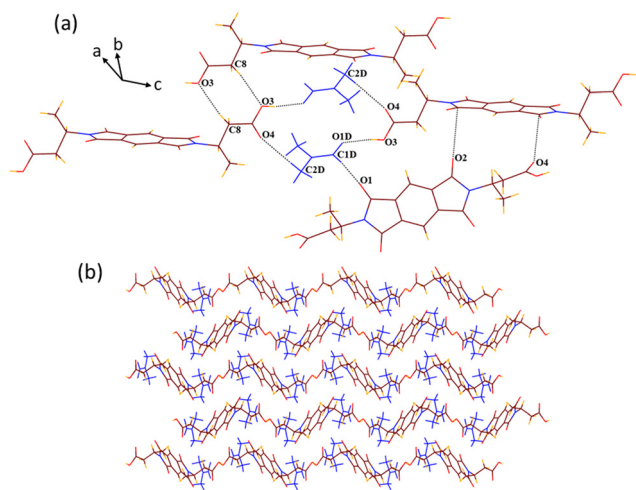
Fig. 1 (a) Part of the crystal lattice of **1a** showing intermolecular host–host and host–guest interactions. (b) A 3D supramolecular host–guest helical network of **1a** (along the *c* axis).
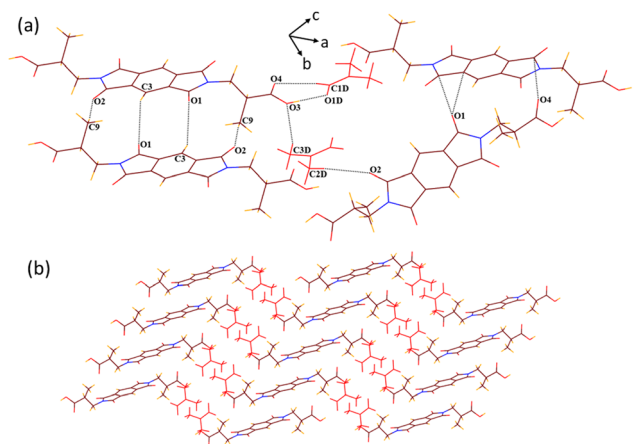

Fig. 2 (a) Various weak interactions in the crystal lattice of **2a**. (b) A 3D zigzag supramolecular architecture of solvate **2a** (along the *b* axis).

These layers of host molecules further interact with each other *via* bifurcated O1···π (3.16 Å) and O4···π (3.029 Å) interactions to construct a 3D zigzag type of host–guest supramolecular architecture accommodating the layers of guest molecules between the layers of host molecules. In the structures of both DMF solvates **1a** and **2a**, no weak interactions among the guest molecules are observed in their crystal lattices.

In the host–guest structures **1a** and **2a**, it is observed that the –COOH group of both the isomeric hosts interacts with two DMF molecules, making different types of hydrogen bond motifs. In the case of structure **1a**, both the DMF molecules interact with the –COOH group *via* discrete C–H···O and O–H···O donor–acceptor interactions (motif **III**; Scheme 1), while in the case of structure **2a**, one DMF molecule interacts with the –COOH group *via* a discrete donor C–H···O interaction and another DMF molecule forms a cyclic $R_2^2(7)$ hydrogen bond by the combination of C–H···O and O–H···O donor–acceptor

interactions (motif **IV**). DFT calculations on analogous motifs constructed from formic acid and DMF are carried out to establish the existence of both types of motifs, as observed in the structures of solvates **1a** and **2a**. The optimized structures of formic acid and DMF motifs at the basis function B3LYP/6-31+G* are shown in Fig. 3.

In structure **3a**, the carbonyl oxygen and methyl hydrogen of two DMF molecules are allowed to form a discrete acceptor O–H···O interaction and a discrete donor C–H···O interaction with a formic acid molecule. In structure **3b**, optimization of a formic acid and two DMF molecules facilitated the formation of a similar discrete donor C–H···O interaction along with two short range donor–acceptor C–H···O and O–H···O interactions. The interaction energies of **3a** and **3b** along with the relative stability of **3b** calculated with different basis functions are shown in Table 1. It is evident from the inspections of crystal structures (**1a** and **2a**) and optimized structures (**3a** and **3b**) that the DMF molecules form two hydrogen bonds with the host in the case of the former, while three hydrogen bonds in
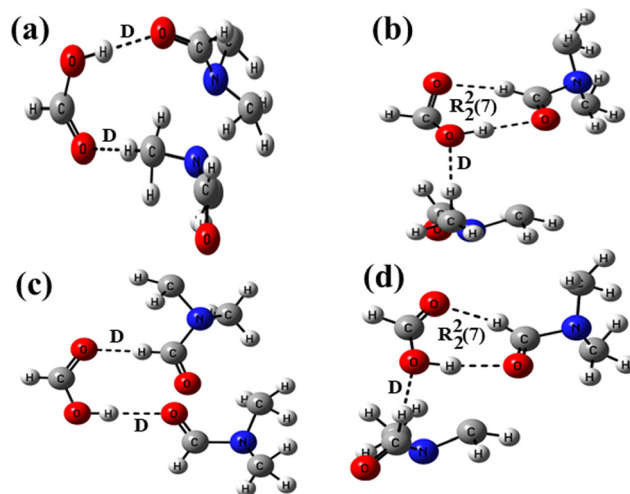

Fig. 3 Optimized structures of formic acid–DMF at the B3LYP/6-31+G* level showing (a) two D motifs, (b) D and $R_2^2(7)$ motifs, (c) two D motifs and (d) D and $R_2^2(7)$ motifs.

Table 1 Calculated interaction energies (E_{int}) at different basis sets and differences in the E_{int} of the optimized structures (in eV)

	Interaction energies (E_{int})		Relative stabilities
Functional/basis sets	**3a**	**3b**	Stability of **3b** over **3a**
B3LYP/6-31+G*	−7.4430	−11.4450	4.0020
B3LYP/6-31++G*	−7.0742	−11.0634	3.9892
B3LYP/6-31+G**	−8.5083	−12.2870	3.7787
AUG-cc-pVDZ	−10.1790	−13.8498	3.6708

	Interaction energies (E_{int})		Relative stabilities
Functional/basis sets	**3c**	**3d**	Stability of **3d** over **3c**
B3LYP/6-31+G*	−6.5270	−11.5357	5.0087
B3LYP/6-31++G*	−6.5626	−12.6610	6.0984
B3LYP/6-31+G**	−7.9430	−12.9110	4.9680
AUG-cc-pVDZ	−9.6022	−14.4675	4.8653

the case of the latter; consequently, structure **3b** was found to be more stable than **3a**. The relative stability of **3b** is found to be higher (4.0 eV) with lower-level basis function B3LYP/ 6-31+G⋆, lowered with higher-level basis functions such as 6-31++G⋆ (3.99 eV) and 6-31+G⋆⋆ (3.78 eV), and is smaller (3.67 eV) with highly polarized and double diffused basis function AUG-cc-pVDZ. The formation of discrete and cyclic $R_2^2(7)$ motifs (**I** and **II** in Scheme 1) in an equal stoichiometric ratio between the –COOH groups of two isomeric hosts and the DMF molecule has recently been studied experimentally and theoretically.[55] Our recently reported and current investigations confirm that the cyclic $R_2^2(7)$ is more stable than the D motif.

We have also designed two other motifs **V** and **VI** (as shown in Scheme 1), which are almost similar to motifs **III** and **IV**, respectively. In these two motifs, the position of one DMF molecule is changed, and it is allowed to create a discrete acceptor C–H···O interaction with the –COOH group *via* α-hydrogen instead of methyl-hydrogen. Because these motifs are not observed in the structures of DMF solvates, the possibility of their formation is also checked by DFT calculations. For this purpose, analogous structures **3c** and **3d** are constructed from formic acid and DMF (Fig. 3), and their interaction energies are calculated at different basis functions (Table 1). Similar to the aforementioned results, structure **3d** is found to be more stable than structure **3c**. The relative stability is found to be the highest (6.09 eV) in the case of basis function 6-31++G⋆ and the lowest (4.86 eV) in the case of basis function AUG-cc-pVDZ. Moreover, to check the relative stabilities of motifs **V** and **VI** with motifs **III** and **IV**, the interaction energies of structures **3a** and **3b** are compared with those of **3c** and **3d**, respectively (Table S1; ESI†). It is observed that structure **3a**, which is analogous to motif **III** and is observed in the structure of solvate **1a**, is more stable than structure **3c**, which is analogous to motif **V** and is not observed in the structures of DMF solvates. Unlikely, structure **3b** is less stable than structure **3d**, showing minor energy differences for each basis set. The stability of **3a** over **3c** is found in the range of 0.51–0.92 eV and the stability of **3d** over **3b** is found in the range of 0.62–1.59 eV, with various levels of functional calculations. The differences in the interaction energies of such alike motifs are negligible. Therefore, it can be concluded that various other weak interactions along with the interaction energies of dissimilar motifs play a crucial role in their formation. The significance of such small interaction energies of slightly different hydrogen bond motifs in the crystal lattice is documented well towards the improvement of chemical and physical properties of multi-component crystalline materials.[56,57]

Solvate **1b** crystallizes in a triclinic $P\bar{1}$ space group as a 1 : 2 host–guest complex containing half of the host molecule and one pyridine guest molecule in its crystallographic asymmetric unit. In the structure of **1b**, all the six hydrogen bonding sites of the guest pyridine molecule make hydrogen bonds with the host molecule (Fig. 4). The guest pyridine molecule binds with the –COOH group of the host molecule *via* the cyclic $R_2^2(7)$ hydrogen bond motif, which is formed by the combination of acceptor–donor OH–N (O3–H3···N1P, $d_{D···A}$ 2.63 Å, ∠ D–H···A 173.6°) and
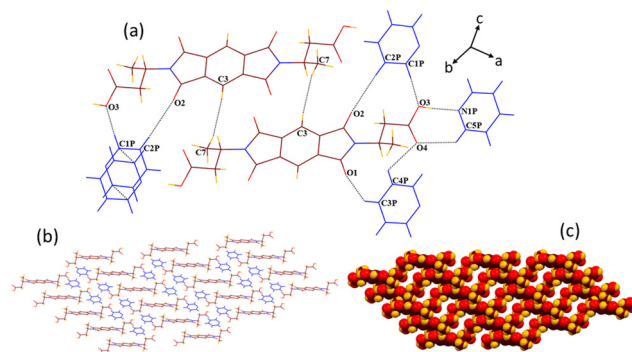

Fig. 4 (a) Intermolecular interactions of the host–guest assembly of **1b**. (b) Formation of tetrameric assemblies of the hosts encapsulating the guests in the crystal lattice of **1b** (along the *b* axis). (c) Space filling model of a 3D channel architecture after removal of guests inside the channels.

CH–O (C5P–H5P···O4, 3.61 Å, 124.7°) interactions. It also interacts with both the oxygen atoms of the –COOH group *via* two discrete CH–O (C1P–H1P···O3, 3.47 Å, 156.6° and C4P–H4P···O4, 3.64 Å, 121.6°) interactions. Moreover, the remaining two hydrogen bonding sites of pyridine engage in the formation of C3P–H3P···O1 (3.41 Å, 136.5°) and C2P–H2P···O2 (3.56 Å, 175.5°) bonds with the carbonyl oxygen atoms of the host molecule, making a 2D host–guest assembly. The host molecules interact with each other *via* short H–H (H3A···H7C, 2.35 Å) contacts to form a 3D channelled architecture, which is sustained by the repeated tetrameric assembly of host molecules as viewed along the *b* axis. The guest pyridine molecules reside inside the channels of 18.06 × 6.40 Å dimensions by interacting with each other *via* π–π (3.37 Å) contacts.

Solvate **2b** crystallizes in the monoclinic $P2_1/c$ space group. A crystallographic asymmetric unit of **2b** includes half of the host molecule and one pyridine guest molecule. In the crystal lattice of **2b**, all the six hydrogen bonding sites and the π-bonding site of the guest pyridine molecule interact with the host molecule (Fig. 5). Compared with the structure of **2a**, guest pyridine similarly interacts with the host by the combination of O3–H3···N1P ($d_{D···A}$ 2.75 Å, ∠ D–H···A 177.1°) and C1P–H1P···O4 (3.12 Å, 129.3°) interactions, making a cyclic $R_2^2(7)$ motif. In contrast to the structure of **2a**, where guest pyridine was found to interact with both the oxygen atoms of the –COOH group *via*
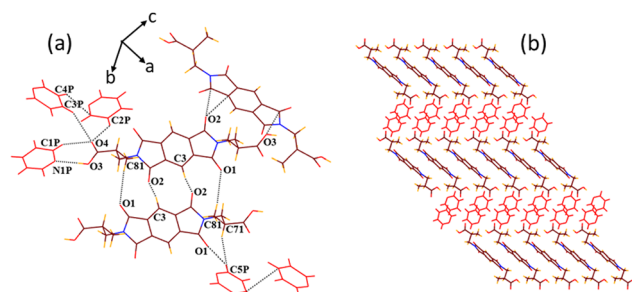

Fig. 5 (a) Various weak interactions in the crystal lattice of **2b**. (b) Formation of a 3D zigzag host–guest structural arrangement in the supramolecular structure of **2b** (along the *b* axis).

two discrete CH–O hydrogen bonds, the guest pyridine makes bifurcated CH–O (C3P–H3P$\cdots$O4, 3.56 Å, 151.7° and C2P–H2P$\cdots$O4, 3.46 Å, 138.6°) contacts with only one oxygen atom of the –COOH group in the structure of **2b**. The formation of one more weak bond C5P–H5P$\cdots$O1 (3.22 Å, 150.9°) also occurs between the guest and carbonyl oxygen of five membered cyclic imide rings of the host. The aromatic ring of the guest molecule interacts with the methylene group of the host *via* a weak C71–H71$\cdots$π (2.87 Å) interaction. Apart from these host–guest interactions, host molecules also interact with each other *via* two types of CH–O (C81–H81$\cdots$O1, 3.67 Å, 168.7° and C3–H3A$\cdots$O2, 3.26 Å, 137.5°) and O–π (O3$\cdots$π, 3.19 Å and O2$\cdots$π, 3.0 Å) interactions. The guest molecules interact with each other *via* C4P–H4P$\cdots$π (2.84 Å) and π–π (3.3 Å) contacts. These interactions result in the formation of a similar type of zigzag 3D supramolecular architecture (along the *b* axis), as observed in the case of DMF solvate **2a**.

The crystal structure analyses of solvates **1b** and **2b** also revealed the formation of distinct motifs between the –COOH groups of hosts and guest pyridine molecules with 1 : 3 stoichiometric ratios in both cases (motifs **IX** and **X** in Scheme 1). The analogous structures of such motifs between the formic acid and pyridine are constructed at the B3LYP/6-31+G* level of the basis function (Fig. 6). In these structures, one pyridine molecule is allowed to form a cyclic $R_2^2(7)$ hydrogen bond by the combination of an acceptor O–H$\cdots$N interaction and a donor C–H$\cdots$O interaction, while the other two pyridine molecules form two discrete donor C–H$\cdots$O interactions with the –COOH group. In structure **6a**, both the carbonyl and the hydroxyl oxygen atoms are involved in discretely binding two pyridine molecules, while in the case of structure **6b**, only the carbonyl oxygen atom is involved in binding two pyridine molecules in a bifurcated manner. The interaction energies and the relative stabilities of these structures are calculated at different basis sets using the B3LYP functional (Table 2). Because structures **6a** and **6b** show almost similar types of binding patterns with four

Table 2 Calculated interaction energies (E_{int}) at different basis sets and differences in the E_{int} of the optimized structures (in eV)

	Interaction energies (E_{int})		Relative stabilities
Functional/basis sets	6a	6b	Stability of 6b over 6a
B3LYP/6-31+G*	−12.4450	−12.4942	0.0492
B3LYP/6-31++G*	−12.4640	−12.9875	0.5235
B3LYP/6-31+G**	−13.2640	−13.2695	0.0055
AUG-cc-pVDZ	−13.6825	−13.6892	0.0067

	Interaction energies (E_{int})		Relative stabilities
Functional/basis sets	6c	6d	Stability of 6d over 6c
B3LYP/6-31+G*	−4.0820	−6.9809	2.8989
B3LYP/6-31++G*	−4.0093	−7.2104	3.2011
B3LYP/6-31+G**	−5.0489	−7.9170	2.8681
AUG-cc-pVDZ	−6.4721	−9.3483	2.8762

hydrogen bonds in each case, the differences in the interaction energies are also small on each basis set, demonstrating that structure **6b** is more stable than structure **6a**.

The interaction energies of two probable motifs, **XI** and **XII**, which are not observed in pyridine solvates **1b** and **2b**, are also calculated to compare the stability of these motifs with motifs **IX** and **X**, respectively. In these motifs, three pyridine molecules are attached to the –COOH group *via* two discrete donor C–H$\cdots$O and one discrete acceptor O–H$\cdots$N bonds. The analogous structures between the formic acid and pyridine molecules are optimized for this purpose at B3LYP/6-31+G* level of basis function (**6c** and **6d** depicted in Fig. 6), and their interaction energies and relative stabilities are calculated at different basis sets (Table 2). The results are similar to the trend observed for structures **6a** and **6b**, showing minor differences in the interaction energies between these structures. However, when the interaction energies of structures **6a** and **6b** are compared with **6c** and **6d**, respectively (Table S2, ESI†), the differences are noteworthy ($\sim$5–8 eV) in determining the higher stability of structures **6a** and **6b** over **6c** and **6d**, respectively, which may be the reason for the formation of motifs **IX** and **X** in pyridine solvates **1b** and **2b**. The DFT calculations of the interaction energies of closely related motifs suggest that the formation of higher stable motifs is more feasible, and minor energy differences in the interaction energies may not impact alterations in hydrogen bond patterns, which are further guided by the presence of other weak interactions in the crystal lattices. The interaction energies of all the model structures between formic acid–DMF and formic acid–pyridine are also calculated at different basis sets of higher level B3LYP-D3 functional (Table S3, ESI†) and are found to follow a similar trend, as it was for different basis sets of functional B3LYP.

Solvate **1c** crystallizes in a triclinic $P\bar{1}$ space group showing half of the host molecule **1** and one guest quinoline molecule in its crystallographic asymmetric unit. In the crystal lattice of **1c**, guest quinoline interacts with the –COOH group of the host molecule only *via* discrete O3–H3$\cdots$N1Q ($d_{D\cdots A}$ 2.65 Å, $\angle$D–H$\cdots$A 173.9°) interaction (Fig. 7). Further, it makes contact with the carbonyl oxygens of the host molecule *via*
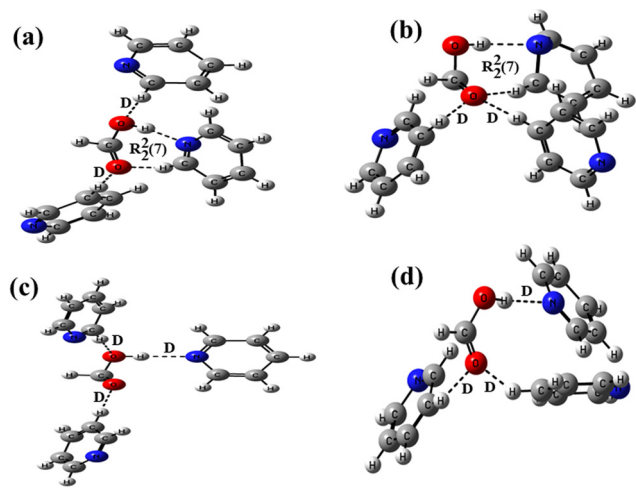

Fig. 6 Optimized structures of formic acid–pyridine at the B3LYP/6-31+G* level making (a) two D and a $R_2^2(7)$ motifs, (b) two D and a $R_2^2(7)$ motifs, (c) three D motifs, and (d) three D motifs.
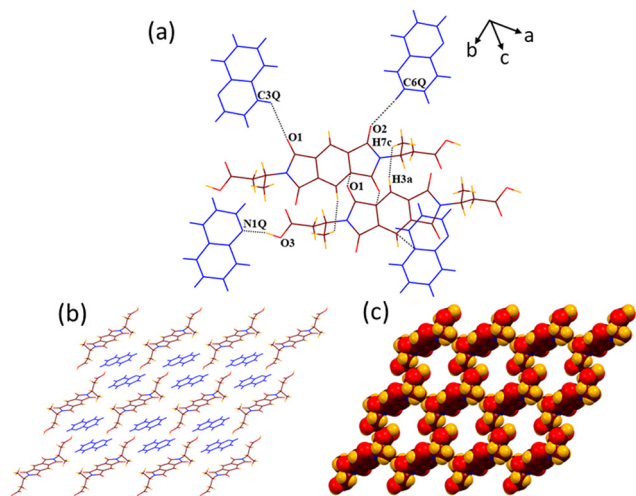
Fig. 7 (a) Part of the crystal structure of **1c** showing different types of weak interactions. (b) Formation of tetrameric assemblies of hosts encapsulating guests in a 3D hydrogen-bonded structure of **1c** (along the *a*-axis). (c) Space filling model after removal of guest quinoline molecules inside the channels.

C3Q–H3Q···O1 (3.3 Å, 122.1°) and C6Q–H6Q···O2 (3.58 Å, 162.9°) interactions and also makes weak π–π (3.26 Å) contact with the aromatic ring of the host molecule. The host molecules interact with each other *via* C=O···π (3.14 Å) and weak H3A–H7C (2.34 Å) contacts. No interactions among the guest molecules are observed in the structure of **1c**. Similar to pyridine solvate **1b**, the 3D supramolecular network of **1c** consists of tetrameric assemblies of host molecules encapsulating the guest molecules inside the channels of 19.7 × 6.6 Å dimension, as viewed along the *a*-axis.

Solvate **2c** crystallizes in the triclinic *P*1̄ space group, and the asymmetric unit of this has one molecule of host **2** and two symmetry non-equivalent guest quinoline molecules. In the crystal lattice of **2c**, both sets of symmetry independent guest quinoline molecules make discrete OH–N (O7–H7···N1Q, $d_{D···A}$ 2.67 Å, ∠D–H···A 154.4° and O5–H5···N2Q, 2.62 Å, 144.3°) contacts with both the –COOH groups of host molecule (Fig. 8). Apart from that, the first set of quinoline molecules (shown as blue) interact with the carbonyl oxygen of host molecule *via* C7Q–H7Q···O4 (3.29 Å, 144.3°) interaction, while the second set of quinoline molecules (shown in red) form two more discrete donor CH–O (C10Q–H10Q···O8, 3.47 Å, 145.6° and C12Q–H12Q···O8 Å, 3.25, 160°) contacts with the –COOH group of the host along with the same type of CH–O (C15Q–H15Q···O1, 3.37 Å, 156.4°) contact, as formed by the first set of guest molecules with the host. The host molecules interact with each other *via* C3–H3···O6 (3.46 Å, 157.2°) and C=O···π (C10–O4···π, 3.17 Å) interactions. Overall, a 3D host–guest channelled architecture is formed along the *b* axis by the combination of the host and second type of guest quinoline molecules. The first type of guest molecules resides inside these channels of approximately 14.8 × 8.8 Å dimensions. Even though the second type of guest molecules form π–π interactions with the host (3.391 Å), no weak interactions among the
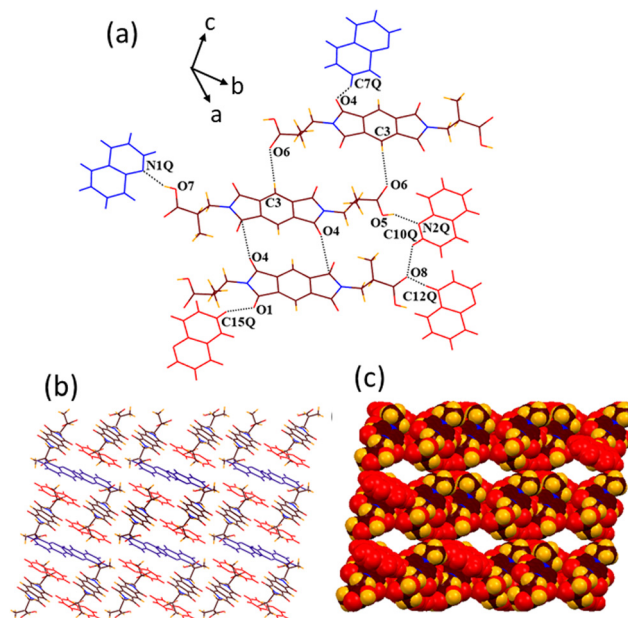

Fig. 8 (a) Various weak interactions between the host and two types of symmetry independent guest molecules in the structure of **2c**. (b) Formation of a 3D supramolecular channel architecture by the combination of host and one type of symmetry independent guest molecule (red) (along the *b* axis). (c) Space filling model after removal of another type of guest molecules (blue) inside the channels.

guest molecules are observed in the supramolecular structure of **2c**.

Solvate **2d** crystallizes in the triclinic *P*1̄ space group, including half molecule of host **2** lying on the inversion centre with half guest quinoline and one guest piperidine molecule in its crystallographic asymmetric unit. Because the host and guest quinoline molecules are found disordered in the structure of **2d**, a better description of hydrogen bonding is not possible. However, the guest piperidine molecules are found to interact with the –COOH group of the host *via* two discrete CH–O (C2P–H2P2···O31, $d_{D···A}$ 2.72 Å, ∠D–H···A 169.5° and C2P–H2P1···O41, 2.67 Å, 157.3°) interactions (Fig. 9). Moreover, two methylene hydrogens of guest piperidine interact with the carbonyl oxygen of the host *via* bifurcated CH–O (C1P–H1P1···O1, 3.59 Å, 170.8° and C4P–H4P1···O1, 3.61 Å, 159°) interactions. A 2D host–guest assembly thus formed by the combination of host and guest piperidine is further converted to a 3D supramolecular channelled architecture *via* C3–H3···O2 (3.28 Å, 127°) host–host interactions. The guest quinoline molecules interact with the hosts only *via* strong π–π (3.38 Å) contacts and reside inside the channels of approximately 9.4 × 19.5 dimensions, as viewed along the *b* axis. No interactions among both types of guest molecules are observed in the crystal lattice of **2d**.

Fluorescence emission, PXRD and thermal analyses

Aromatic imides are a class of important π-conjugated organic luminescent materials used in optoelectronics due to their rigid structures, excellent photochemical and thermal stabilities,
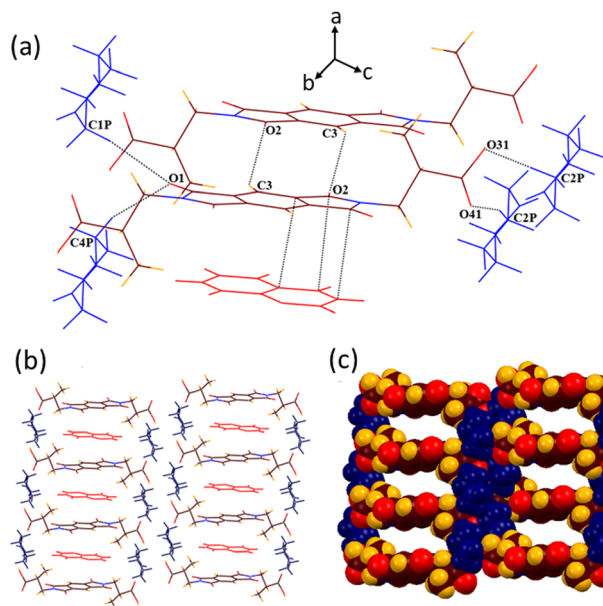
Fig. 9 (a) Intermolecular interactions in the host–guest assembly of **2d**. (b) Formation of 3D supramolecular channel network by the combination of hosts and guest piperidine molecules accommodating guest quinoline molecules (along the *b* axis). (c) Space filling model after the removal of guest quinoline molecules inside the channels.

high fluorescence quantum yields and good electron transmission abilities. In particular, aromatic cyclic imides, such as PMDI and NDI, exhibited remarkable contributions in a wide range of applications, including organic light-emitting diodes,[58] organic field-effect transistors,[59] organic solar cells,[60] chemosensors,[61] and bioprobes.[62] Such types of π-conjugated small organic emitters have been reported to exhibit emissions in the blue spectral region.

In view of their potential applications, the solid state fluorescence emission properties of both the host compounds along with their solvates are recorded. All these materials are found to show emissions in the blue spectral region (Fig. 10). Upon excitation at 340 nm, host **1** and its DMF solvate **1a** show similar emission patterns with an emission peak at 455 nm along with two shoulder peaks at 400 and 485 nm, respectively.

However, major differences are observed between the emission spectra of host **1** and its pyridine and quinoline solvates (**1b** and **1c**). Solvates **1b** and **1c** show highly intense emission peaks at 410 and 450 nm, respectively. It should be noted that along with the intensity of emission peaks, the emission of pyridine solvate **1b** appears to be blue shifted at ~40–45 nm in comparison to the emissions of host **1** and its other solvates (Fig. 10a).

Similarly, upon excitation at 340 nm, the emission spectra of host **2** and its DMF solvate **2a** also appear to resemble each other, with the spectra of host **1** and its DMF solvate **1a**, respectively. The emission spectrum of pyridine solvate **2b** is also similar to the host and its DMF solvates except showing a comparatively more intense blue-shifted peak at 400 nm. Similar to the quinoline solvate of host **1**, strong emission peaks for quinoline solvate **2c** and mixed quinoline/piperidine solvate **2d** of host **2** are also obtained in the 445–455 nm region (Fig. 10b). To directly compare the variations in emission wavelengths of these samples, normalised emission spectra of both the hosts and their solvates, along with the photographs of emissive materials in the ground state, are shown in Fig. S5 and S6 (ESI†), respectively. Because the emission spectra of all the solvates are recorded in the solid state, the relative quantum yields for these systems could not be achieved.

It is quite obvious from the structural investigations of all solvates that the 3D supramolecular architectures of pyridine and quinoline solvates, namely, **1b**, **1c**, **2c** and **2d**, are moderately different from other solvates showing intense emissions. In the structures of these solvates, the size of guest molecules as well as minor differences in the weak interactions changes the packing pattern, and the formation of porous architectures occurs containing channels and cavities of different dimensions accommodating the guest molecules inside them. The structures of other DMF and pyridine solvates, namely, **1a**, **2a** and **2b**, show tight-packed 3D layered architectures of hosts and guests with no channels and cavities. Therefore, the differences in the emission spectra are probably due to changes in the host–guest supramolecular arrangements in the solid crystalline phases. It has been demonstrated that the emissive properties of materials can be tuned from lower to higher by increasing the porosity of supramolecular aggregates.[63]
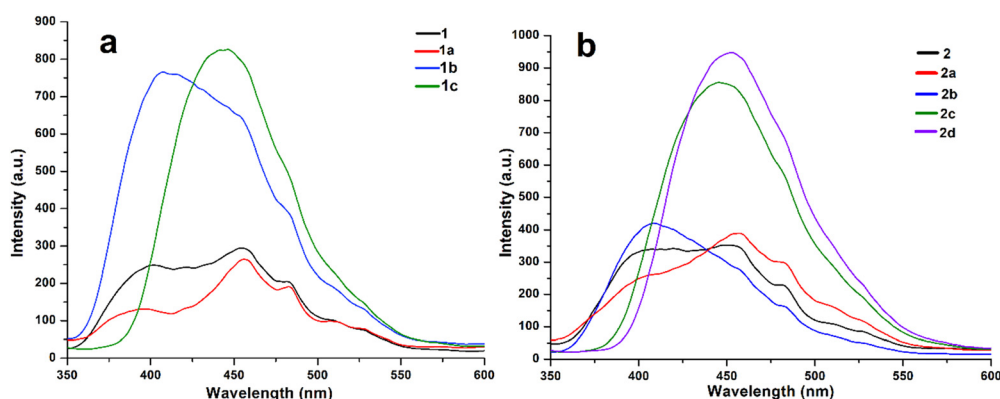

Fig. 10 Solid state fluorescence emission spectra of (a) host **1** and its solvates **1a**, **1b** and **1c** and (b) host **2** and its solvates **2a**, **2b**, **2c** and **2d**.

Moreover, extending the conjugated backbone of aromatic imides or adding a π-conjugated guest by cooperative donor–acceptor interactions is an efficient way to enhance luminescence efficiency. It is also evident from the crystal structure inspections that the photoluminescence of the solvates with aromatic guests is found to increase 2–3 fold due to the aggregation-induced emission enhancement (AIEE), which is attributed to the strong π–π interactions between the electron deficient PMDI hosts and electron rich aromatic guests. It has been established that strong π–π stacking in a solid state can deactivate the non-radiative decay pathway, leading to a longer lifetime of luminescent materials, and is the main cause for enhanced emission behaviour.[64] Such photoluminescence enhancements originate from the emissive exciplex or the excited electronic intermolecular charge transfer state formed by the hosts and aromatic guest molecules in the crystals.[65] The photoluminescence enhancement of a metal NDI framework is revealed by the formation of an exciplex electronic charge transfer state between the framework and electron rich naphthalene guest molecules.[66] It has already been reported that the photoluminescence of electron deficient NDI hosts can be enhanced by the interaction with π-electron rich aromatic systems through a charge-transfer excitation mechanism.[67]

Notably, the emission spectra of pyridine solvates **1b** and **2b** appear to be blue shifted (∼40–50 nm) compared with the other solvates of hosts **1** and **2**, e.g., DMF solvates **1a** and **2a**, respectively. Alternatively, the energies of the FMOs of the formic acid–DMF and formic acid–pyridine model structures are considered to justify the blue-shifted luminescence of solvates **1b** and **2b**. The theoretical band gaps between the LUMO and HOMO of model structures **3a** and **6a** as well as **3b** and **6b**, respectively, are calculated and compared with each other (Fig. 11). The higher band gap (2.58 eV) between the LUMO and HOMO of structure **6a** than the band gap (1.29 eV) between the LUMO and HOMO of structure **3a** suggested a lower emission wavelength for solvate **1b** than for solvate **1a** (Fig. 11a). Similarly, the higher band gap (1.46 eV) between the LUMO and HOMO of structure **6b** than the band gap (0.75 eV) between the LUMO and HOMO of structure **3b** suggested a lower emission wavelength for solvate **2b** than for

solvate **2a** (Fig. 11b). According to the FMO theory, a higher band gap between the LUMO and HOMO implies a higher energy requirement for electronic transition, suggesting that the material emits light at shorter wavelength.[68] The guest-dependent emission variations in the crystals of multimolecular hydrogen-bonded systems via guest–host donor–acceptor interactions have also been reported by Hisaeda's group.[67]

The PXRD patterns of all host–guest crystalline materials are recorded along with their host compounds to check the phase purity of bulk samples. The differences in the PXRD peaks of the individual host and its various complexes are clearly visible due to the presence of different guest solvent molecules in the crystal lattice of each host–guest complex (Fig. 12). The peaks obtained in the experimental PXRD patterns of all the complexes are found to correlate well with the peaks of their simulated patterns from SCXRD (Fig. S7–S13, ESI†). However, some small deviations among the theoretical and experimental peaks are attributed to the loss of solvent molecules from the solvates, leading to the loss of crystallinity.[39,51]

To examine the stabilities and host–guest stoichiometries, TGA and DSC analyses of all the host–guest complexes are carried out (Fig. S14–S20, ESI†). The TGA curve of solvate **1a** shows that it loses both the guest DMF molecules in one step (exp. 25.15% weight) in the temperature range of 50–100 °C (calcd 27.3%). A sharp endothermic peak appears at 85 °C for the loss of solvent molecules in its DSC profile. Solvate **1b** also loses two guest pyridine molecules in a single step between 55 and 115 °C, showing a sharp endotherm in DSC at 110 °C (exp. 29.6%, calcd 28.9%). Solvate **1c** similarly loses two guest quinoline molecules in the 115–165 °C temperature range, for which an endothermic peak appears at 152 °C in the DSC profile (exp. 40.13%, calcd 39.93%).

Solvate **2a** loses two guest DMF molecules between 55 and 90 °C in one step, showing a sharp peak at 85 °C in the DSC curve (exp. 28.08%, calcd 27.3%). Solvate **2b** starts losing guest molecules in one step as the temperature increases above the room temperature and ends at 110 °C, showing a sharp endothermic peak at 70 °C (exp. 22.9%, calcd 28.9%). Solvate **2c** loses two quinolines in the 110–180 °C temperature range, showing two endothermic peaks at 120 and 155 °C for
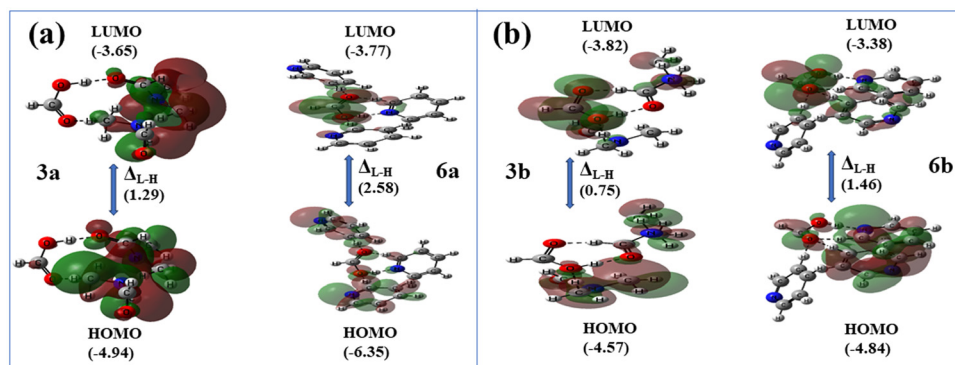

Fig. 11 Optimized Frontier molecular orbitals and orbital energies (in eV) of structures (a) **3a** and **6a** and (b) **3b** and **6b** via DFT at the B3LYP/6-31+G* level.
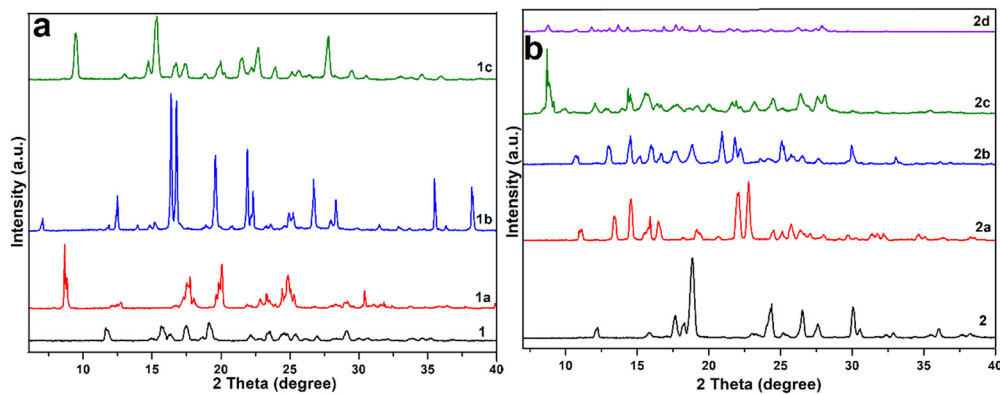
Fig. 12 PXRD patterns of (a) host **1** and its solvates **1a**, **1b** and **1c** and (b) host **2** and its solvates **2a**, **2b**, **2c** and **2d**.

successive loss of two symmetry non-equivalent guest quinolines due to their different binding tendencies with the host (exp. 42.3%, calcd 39.93%). A single step weight loss for two piperidine and one quinoline guest molecule in the temperature range of 80–130 °C is observed for solvate **2d** in the TGA curve with an endothermic peak at 125 °C in the DSC curve (exp. 40.13%, calcd 45%).

Conclusions

In this work, the attachment of multiple solvent molecules with the –COOH group of two isomeric pyromellitic diimide host molecules showing diverse interactions is assessed. The role of various intermolecular interactions in the construction of 3D supramolecular host–guest frameworks is discussed along with their varying photoluminescence behaviour. In the crystal lattices of DMF solvates **1a** and **2a**, both DMF guests are attached to the –COOH groups of hosts *via* two D motifs and *via* one R motif and one D motif, respectively. In pyridine solvates **1b** and **2b**, three pyridine molecules are also attached with –COOH groups of hosts having different combinations of hydrogen bonds, *viz.*, *via* two dissimilar types of D and one R and *via* two similar types of D and one R motifs, respectively. In quinoline solvates **1c** and **2c**, quinoline molecules are attached with the –COOH groups *via* a similar D motif, while no interaction of guest quinoline with the host is observed in the case of mixed solvate **2d**. Both the experimental and theoretical estimations are carried out to analyse the formation of some new and distinct hydrogen bond motifs between the two similar host–guest binding entities. The possibility of the formation of some other closely related motifs between the identical host and guest with the same number of donor/acceptor groups, as observed in the structures of solvates, is also supported by the results of the DFT calculations. The variations in the photophysical properties of hydrogen-bonded frameworks are closely associated with the energy differences between the HOMO and LUMO of the designed model synthons. It is concluded that minor differences in the interaction energies may not restrict the formation of such diverse motifs between the same binding entities, and the

formation of either motif depends on the geometric alignment of the host and other host–guest weak interactions in the crystal lattices. However, major differences in the interaction energies of hydrogen bond patterns may result in desired molecular arrangements, leading to changes in physicochemical properties and potential applications of multi-component hydrogen-bonded solids, such as pharmaceuticals, agrochemicals, biomedicals, and optical materials.

Author contributions

R. R. Puniya, P. Takhar and M. Chhapoliya performed the experiments and analysed the data. R. Deka and D. J. Kalita performed DFT calculations. D. Singh wrote the manuscript and approved the final version with the contributions of all authors.

Data availability

The data supporting this article are available in the ESI.† Crystallographic data for this paper have been deposited at the Cambridge Crystallographic Data Centre (CCDC) under deposition number 2324804–2324810.†

Conflicts of interest

There are no conflicts to declare.

References

1 D. Venkataraman, S. Lee, J. Zhang and J. S. Moore, An organic solid with wide channels based on hydrogen bonding between macrocycles, *Nature*, 1994, **371**, 591–593.

2 M. E. Davis, Ordered porous materials for emerging applications, *Nature*, 2002, **417**, 813–821.

3 R.-B. Lin, Y. He, P. Li, H. Wang, W. Zhou and B. Chen, Multifunctional porous hydrogen-bonded organic framework materials, *Chem. Soc. Rev.*, 2019, **48**, 1362–1389.

4 T.-U. Yoon, S. B. Baek, D. Kim, E.-J. Kim, W.-G. Lee, B. K. Singh, M. S. Lah, Y.-S. Bae and K. S. Kim, Efficient separation of C_2 hydrocarbons in a permanently porous hydrogen-bonded organic framework, *Chem. Commun.*, 2018, **54**, 9360–9363.

5 M. Simard, D. Su and J. D. Wuest, Use of hydrogen bonds to control molecular aggregation. Self-assembly of three-dimensional networks with large chambers, *J. Am. Chem. Soc.*, 1991, **113**, 4696–4698.

6 S. Tsuzuki, K. Honda, T. Uchimaru, M. Mikami and K. Tanabe, Origin of attraction and directionality of the π/π interaction: model chemistry calculations of benzene dimer interaction, *J. Am. Chem. Soc.*, 2002, **124**, 104–112.

7 I. Hisaki, S. Nakagawa, N. Ikenaka, Y. Imamura, M. Katouda, M. Tashiro, H. Tsuchida, T. Ogoshi, H. Sato, N. Tohnai and M. Miyata, A series of layered assemblies of hydrogen-bonded, hexagonal networks of C_3-symmetric π-conjugated molecules: a potential motif of porous organic materials, *J. Am. Chem. Soc.*, 2016, **138**, 6617–6628.

8 P. Wei, X. He, Z. Zheng, D. He, Q. Li, J. Gong, J. Zhang, H. H. Y. Sung, I. D. Williams, J. W. Y. Lam, M. Liu and B. Z. Tang, Robust supramolecular nano-tunnels built from molecular bricks, *Angew. Chem., Int. Ed.*, 2021, **60**, 7148–7154.

9 W. Yang, A. Greenaway, X. Lin, R. Matsuda, A. J. Blake, C. Wilson, W. Lewis, P. Hubberstey, S. Kitagawa, N. R. Champness and M. Schröder, Exceptional thermal stability in a supramolecular organic framework: porosity and gas storage, *J. Am. Chem. Soc.*, 2010, **132**, 14457–14469.

10 S. Yu, G.-L. Xing, L.-H. Chen, T. Ben and B.-L. Su, Crystalline porous organic salts: from micropore to hierarchical pores, *Adv. Mater.*, 2020, **32**, 2003270.

11 J. Liang, S. Xing, P. Brandt, A. Nuhnen, C. Schlüsener, Y. Sun and C. Janiak, A chemically stable cucurbit[6]uril-based hydrogen-bonded organic framework for potential SO_2/CO_2 separation, *J. Mater. Chem. A*, 2020, **8**, 19799–19804.

12 H. Wang, Z. Bao, H. Wu, R.-B. Lin, W. Zhou, T.-L. Hu, B. Li, J. C.-G. Zhao and B. Chen, Two solvent-induced porous hydrogen-bonded organic frameworks: solvent effects on structures and functionalities, *Chem. Commun.*, 2017, **53**, 11150–11153.

13 S. Cai, H. Shi, Z. Zhang, X. Wang, H. Ma, N. Gan, Q. Wu, Z. Cheng, K. Ling, M. Gu, C. Ma, L. Gu, Z. An and W. Huang, Hydrogen-bonded organic aromatic frameworks for ultralong phosphorescence by intralayer π–π interactions, *Angew. Chem., Int. Ed.*, 2018, **57**, 4005–4009.

14 B. Wang, R. He, L.-H. Xie, Z.-J. Lin, X. Zhang, J. Wang, H. Huang, Z. Zhang, K. S. Schanze, J. Zhang, S. Xiang and B. Chen, Microporous hydrogen-bonded organic framework for highly efficient turn-up fluorescent sensing of aniline, *J. Am. Chem. Soc.*, 2020, **142**, 12478–12485.

15 Y. Tang, M. Yuan, B. Jiang, Y. Xiao, Y. Fu, S. Chen, Z. Deng, Q. Pan, C. Tian and H. Fu, Inorganic acid-derived hydrogen-bonded organic frameworks to form nitrogen-rich carbon nitrides for photocatalytic hydrogen evolution, *J. Mater. Chem. A*, 2017, **5**, 21979–21985.

16 B. Han, H. Wang, C. Wang, H. Wu, W. Zhou, B. Chen and J. Jiang, Postsynthetic metalation of a robust hydrogen-bonded organic framework for heterogeneous catalysis, *J. Am. Chem. Soc.*, 2019, **141**, 8737–8740.

17 F. Q. Liu, J. W. Liu, Z. Gao, L. Wang, X.-Z. Fu, L. X. Yang, Y. Tao, W. H. Yin and F. Luo, Constructing bimetal-complex based hydrogen-bonded framework for highly efficient electrocatalytic water splitting, *Appl. Catal., B*, 2019, **258**, 117973.

18 A. Karmakar, R. Illathvalappil, B. Anothumakkool, A. Sen, P. Samanta, A. V. Desai, S. Kurungot and S. K. Ghosh, Hydrogen-bonded organic frameworks (HOFs): a new class of porous crystalline proton-conducting materials, *Angew. Chem., Int. Ed.*, 2016, **55**, 10667–10671.

19 Y. Wang, M. Zhang, Q. Yang, J. Yin, D. Liu, Y. Shang, Z. Kang, R. Wang, D. Sun and J. Jiang, Single-crystal-to-single-crystal transformation and proton conductivity of three hydrogen-bonded organic frameworks, *Chem. Commun.*, 2020, **56**, 15529–15532.

20 W. Liang, F. Carraro, M. B. Solomon, S. G. Bell, H. Amenitsch, C. J. Sumby, N. G. White, P. Falcaro and C. J. Doonan, Enzyme encapsulation in a porous hydrogen-bonded organic framework, *J. Am. Chem. Soc.*, 2019, **141**, 14298–14305.

21 X.-T. He, Y.-H. Luo, D.-L. Hong, F.-H. Chen, Z.-Y. Zheng, C. Wang, J.-Y. Wang, C. Chen and B.-W. Sun, Atomically thin nanoribbons by exfoliation of hydrogen-bonded organic frameworks for drug delivery, *ACS Appl. Nano Mater.*, 2019, **2**, 2437–2445.

22 I. Hisaki, C. Xin, K. Takahashi and T. Nakamura, Designing hydrogen-bonded organic frameworks (HOFs) with permanent porosity, *Angew. Chem., Int. Ed.*, 2019, **58**, 11160–11170.

23 B. Wang, R.-B. Lin, Z. Zhang, S. Xiang and B. Chen, Hydrogen-bonded organic frameworks as a tunable platform for functional materials, *J. Am. Chem. Soc.*, 2020, **142**, 14399–14416.

24 Y. He, S. Xiang and B. Chen, A microporous hydrogen-bonded organic framework for highly selective C_2H_2/C_2H_4 separation at ambient temperature, *J. Am. Chem. Soc.*, 2011, **133**, 14570–14573.

25 M. R. di Nunzio, I. Hisaki and A. Douhal, HOFs under light: relevance to photon-based science and applications, *J. Photochem. Photobiol., C*, 2021, **47**, 100418.

26 N. K. Duggirala, M. L. Perry, Ö. Almarsson and M. J. Zaworotko, Pharmaceutical cocrystals: along the path to improved medicines, *Chem. Commun.*, 2016, **52**, 640–655.

27 F. Hu, C. Liu, M. Wu, J. Pang, F. Jiang, D. Yuan and M. Hong, An ultrastable and easily regenerated hydrogen-bonded organic molecular framework with permanent porosity, *Angew. Chem., Int. Ed.*, 2017, **56**, 2101–2104.

28 N. A. Mir, R. Dubey and G. R. Desiraju, Strategy and methodology in the synthesis of multicomponent molecular solids: the quest for higher cocrystals, *Acc. Chem. Res.*, 2019, **52**, 2210–2220.

29 O. Ermer, Five-Fold Diamond Structure of Adamantane-1,3,5,7-Tetracarboxylic Acid, *J. Am. Chem. Soc.*, 1988, **110**, 3747–3754.

30 V. A. Russell, M. C. Etter and M. D. Ward, Layered materials by molecular design: structural enforcement by hydrogen bonding in guanidinium alkane- and arenesulfonates, *J. Am. Chem. Soc.*, 1994, **116**, 1941–1952.

31 A. Comotti, S. Bracco, A. Yamamoto, M. Beretta, T. Hirukawa, N. Tohnai, M. Miyata and P. Sozzani, Engineering switchable rotors in molecular crystals with open porosity, *J. Am. Chem. Soc.*, 2014, **136**, 618–621.

32 G. Xing, I. Bassanetti, S. Bracco, M. Negroni, C. Bezuidenhout, T. Ben, P. Sozzani and A. Comotti, A double helix of opposite charges to form channels with unique CO_2 selectivity and dynamics, *Chem. Sci.*, 2019, **10**, 730–736.

33 K. E. Maly, E. Gagnon, T. Maris and J. D. Wuest, Engineering hydrogen-bonded molecular crystals built from derivatives of hexaphenylbenzene and related compounds, *J. Am. Chem. Soc.*, 2007, **129**, 4306–4322.

34 M. Mastalerz and I. M. Oppel, Rational construction of an extrinsic porous molecular crystal with an extraordinary high specific surface area, *Angew. Chem., Int. Ed.*, 2012, **51**, 5252–5255.

35 T.-H. Chen, I. Popov, W. Kaveevivitchai, Y.-C. Chuang, Y.-S. Chen, O. Daugulis, A. J. Jacobson and O. S. Miljanić, Thermally robust and porous noncovalent organic framework with high affinity for fluorocarbons and CFCs, *Nat. Commun.*, 2014, **5**, 5131.

36 W. Yang, A. Greenaway, X. Lin, R. Matsuda, A. J. Blake, C. Wilson, W. Lewis, P. Hubberstey, S. Kitagawa, N. R. Champness and M. Schröder, Exceptional thermal stability in a supramolecular organic framework: porosity and gas storage, *J. Am. Chem. Soc.*, 2010, **132**, 14457–14469.

37 H. Zhou, Q. Ye, X. Wu, J. Song, C. M. Cho, Y. Zong, B. Z. Tang, T. S. A. Hor, E. K. L. Yeow and J. Xu, A thermally stable and reversible microporous hydrogen-bonded organic framework: aggregation induced emission and metal ion-sensing properties, *J. Mater. Chem. C*, 2015, **3**, 11874–11880.

38 D. Singh, P. K. Bhattacharyya and J. B. Baruah, Structural studies on solvates of cyclic imide tethered carboxylic acids with pyridine and quinoline, *Cryst. Growth Des.*, 2010, **10**, 348–356.

39 D. Singh and J. B. Baruah, Metal(II) complexes derived from conformation flexible cyclic imide tethered carboxylic acids: syntheses, supramolecular structures, and molecular properties, *Cryst. Growth Des.*, 2012, **12**, 2109–2121.

40 D. Singh and J. B. Baruah, Molecular complex from two different binuclear copper 1,4,5,8-naphthalenetetracarboxylate complexes, *Inorg. Chim. Acta*, 2012, **390**, 37–40.

41 D. Singh and J. B. Baruah, Varieties in symmetry non-equivalent structural arrangements in solvates of 2-(3-methylene-1,3,7-trioxo-6-(2-carboxy-phenyl)-3,5,6,7-tetrahydro-1*H*-pyrrolo[3,4-*f*]isoindol-2-yl)benzoic acid, *J. Mol. Struct.*, 2009, **937**, 75–80.

42 G. Bolla and A. Nangia, Pharmaceutical cocrystals: walking the talk, *Chem. Commun.*, 2016, **52**, 8342–8360.

43 X.-Z. Luo, X.-J. Jia, J.-H. Deng, J.-L. Zhong, H.-J. Liu, K.-J. Wang and D.-C. Zhong, A microporous hydrogen-bonded organic framework: exceptional stability and highly selective adsorption of gas and liquid, *J. Am. Chem. Soc.*, 2013, **135**, 11684–11687.

44 W. Gong, D. Chu, H. Jiang, X. Chen, Y. Cui and Y. Liu, Permanent porous hydrogen-bonded frameworks with two types of Brønsted acid sites for heterogeneous asymmetric catalysis, *Nat. Commun.*, 2019, **10**, 600.

45 Z. Sun, Y. Li, L. Chen, X. Jing and Z. Xie, Fluorescent hydrogen-bonded organic framework for sensing of aromatic compounds, *Cryst. Growth Des.*, 2015, **15**, 542–545.

46 P. Li, Y. He, J. Guang, L. Weng, J. C.-G. Zhao, S. Xiang and B. Chen, A homochiral microporous hydrogen-bonded organic framework for highly enantioselective separation of secondary alcohols, *J. Am. Chem. Soc.*, 2014, **136**, 547–549.

47 G. Xia, Z. Jiang, S. Shen, K. Liang, Q. Shao, Z. Cong and H. Wang, Reversible specific vapoluminescence behavior in pure organic crystals through hydrogen-bonding docking strategy, *Adv. Opt. Mater.*, 2019, **7**, 1801549.

48 M. Wehner, M. I. S. Röhr, M. Bühler, V. Stepanenko, W. Wagner and F. Würthner, Supramolecular polymorphism in one-dimensional self-assembly by kinetic pathway control, *J. Am. Chem. Soc.*, 2019, **141**, 6092–6107.

49 G. D. Pantoş, P. Pengo and J. K. M. Sanders, Hydrogen-bonded helical organic nanotubes, *Angew. Chem., Int. Ed.*, 2007, **46**, 194–197.

50 D. Singh and J. B. Baruah, Solvation controlling reaction paths and gel-formation in imide derivatives, *Tetrahedron Lett.*, 2008, **49**, 4374–4377.

51 D. Singh and J. B. Baruah, Solid state assemblies of cyclic imides tethered hydroxy benzoic acids with pyridine and quinoline: toward the formation of channels and cavities, *Cryst. Growth Des.*, 2012, **12**, 3169–3180.

52 D. Singh and J. B. Baruah, Structural study on solvates of dopamine-based cyclic imide derivatives, *Cryst. Growth Des.*, 2011, **11**, 768–777.

53 D. Singh and J. B. Baruah, Different solvates of two isomeric dicarboxylic acids with pyridine and quinoline, *CrystEngComm*, 2009, **11**, 2688–2694.

54 N. Barooah, R. J. Sarma and J. B. Baruah, Solid-state hydrogen bonded assembly of N,N'-bis(glycinyl)-pyromellitic diimide with aromatic guests, *CrystEngComm*, 2006, **8**, 608–615.

55 R. R. Puniya, P. Takhar, T. Kalita, D. J. Kalita and D. Singh, Design and Development of Hydrogen Bonded Molecular Assemblies Based on Pyromellitic Diimide Tethered Carboxylic Acids as Optical Materials, *Mol. Syst. Des. Eng.*, 2023, **8**, 929–941.

56 M. Igarashi, T. Nozawa, T. Matsumoto, F. Yagihashi, T. Kikuchi and K. Sato, Parallel-stacked aromatic molecules in hydrogen-bonded inorganic frameworks, *Nat. Commun.*, 2021, **12**, 7025.

57 Y. Liu, L. Wang, L. Zhao, Y. Zhang, Z.-T. Li and F. Huang, Multiple hydrogen bonding driven supramolecular architectures and their biomedical applications, *Chem. Soc. Rev.*, 2024, **53**, 1592–1623.

58 H. F. Higginbotham, P. Pander, R. Rybakiewicz, M. K. Etherington, S. Maniam, M. Zagorska, A. Pron, A. P. Monkman and P. Data, Triphenylamine disubstituted naphthalene diimide: elucidation of excited states involved in TADF and application in near-infrared organic light emitting diodes, *J. Mater. Chem. C*, 2018, **6**, 8219–8225.

59 H. Ran, X. Duan, R. Zheng, F. Xie, L. Chen, Z. Zhao, R. Han, Z. Lei and J.-Y. Hu, Two isomeric azulene-decorated naphthodithiophene diimide-based triads: molecular orbital distribution controls polarity change of OFETs through connection position, *ACS Appl. Mater. Interfaces*, 2020, **12**, 23225–23235.

60 M. A. Jameel, T. C.-J. Yang, G. J. Wilson, R. A. Evans, A. Gupta and S. J. Langford, Naphthalene diimide-based electron transport materials for perovskite solar cells, *J. Mater. Chem. A*, 2021, **9**, 27170–27192.

61 Y. Yang, Q. Zhao, W. Feng and F. Li, Luminescent chemodosimeters for bioimaging, *Chem. Rev.*, 2013, **113**, 192–270.

62 B. Zhang, C. Ge, J. Yao, Y. Liu, H. Xie and J. Fang, Selective selenol fluorescent probes: design, synthesis, structural determinants, and biological applications, *J. Am. Chem. Soc.*, 2015, **137**, 757–769.

63 C. M. Carbonaro, S. V. Thakkar, R. Ludmerczki, C. Olla, A. Pinna, D. Loche, L. Malfatti, F. Cesare Marincola and M. F. Casula, How porosity affects the emission of fluorescent carbon dot-silica porous composites, *Microporous Mesoporous Mater.*, 2020, **305**, 110302.

64 J. Yang, X. Zhen, B. Wang, X. Gao, Z. Ren, J. Wang, Y. Xie, J. Li, Q. Peng, K. Pu and Z. Li, The influence of the molecular packing on the room temperature phosphorescence of purely organic luminogens, *Nat. Commun.*, 2018, **9**, 840.

65 T. Ono, A. Taema, A. Goto and Y. Hisaeda, Switching of monomer fluorescence, charge-transfer fluorescence, and room-temperature phosphorescence induced by aromatic guest inclusion in a supramolecular host, *Chem. – Eur. J.*, 2018, **66**, 17487–17496.

66 J.-J. Liu, Y.-B. Shan, C.-R. Fan, M.-J. Lin, C.-C. Huang and W.-X. Dai, Encapsulating naphthalene in an electron-deficient MOF to enhance fluorescence for organic amines sensing, *Inorg. Chem.*, 2016, **55**, 3680–3684.

67 T. Ono, M. Sugimoto and Y. Hisaeda, Multicomponent molecular puzzles for photofunction design: emission color variation in Lewis acid–base pair crystals coupled with guest-to-host charge transfer excitation, *J. Am. Chem. Soc.*, 2015, **137**, 9519–9522.

68 J. Yu, X. Yong, Z. Tang, B. Yang and S. Lu, Theoretical understanding of structure–property relationships in luminescence of carbon dots, *J. Phys. Chem. Lett.*, 2021, **12**, 7671–7687.